Features of the core–valence luminescence and electron energy band structure of $A_{1-x}Cs_xCaCl_3$ (A = K,Rb) crystals

2007 J. Phys.: Condens. Matter 19 476211

(http://iopscience.iop.org/0953-8984/19/47/476211)

IOP PUBLISHING JOURNAL OF PHYSICS: CONDENSED MATTER

J. Phys.: Condens. Matter **19** (2007) 476211 (8pp) doi:10.1088/0953-8984/19/47/476211

Features of the core–valence luminescence and electron energy band structure of $A_{1-x}Cs_xCaCl_3$ (A = K, Rb) crystals

Ya Chornodolskyy[1], G Stryganyuk[1,2], S Syrotyuk[3], A Voloshinovskii[1] and P Rodnyi[4]

[1] Ivan Franko National University of Lviv, 8 Kyryla i Mefodiya Street, 79005 Lviv, Ukraine
[2] Hamburger Synchrotronstrahlungslabor HASYLAB at Deutsches Elektronensynchrotron DESY, Notkestraße 85, 22607 Hamburg, Germany
[3] Lviv Polytechnic National University, 12, S Bandery Street, 79013 Lviv, Ukraine
[4] St Petersburg State Polytechnical University, 29 Polytechnicheskaya Street, 195251 Petersburg, Russia

Received 7 June 2007, in final form 12 September 2007
Published 1 November 2007
Online at stacks.iop.org/JPhysCM/19/476211

Abstract

From luminescence spectroscopy of $CsCaCl_3$, $Rb_{1-x}Cs_xCaCl_3$ and $K_{1-x}Cs_xCaCl_3$ crystals, we have found evidence for intrinsic and impurity core–valence luminescence due to the radiative recombination of valence electrons with the holes of intrinsic or impurity 5p Cs^+ core states. The structural similarity of core–valence luminescence spectra has been revealed for the $A_{1-x}Cs_xCaCl_3$ (A = K, Rb) crystals investigated. The electron energy structure of the $CsCaCl_3$ crystal has been calculated using the pseudopotential approach taking into account the gradient corrections for the exchange–correlation energy. The calculated density of the electronic states of $CsCaCl_3$ has been compared with corresponding parameters obtained from the analysis of core–valence luminescence spectra.

1. Introduction

The radiative recombination of valence electrons with core holes appears in some halide crystals upon high energy excitation sufficient for outermost core state ionization. This kind of intrinsic emission is known as core–valence luminescence (CVL) [1], cross-luminescence [2], Auger-free luminescence [3]. Figure 1(a) presents a simplified energy band scheme together with the absorption and radiative transitions causing the core–valence luminescence in the wide-band halide crystals. The CVL features provide the possibility of determining the parameters of the energy band structure for the CVL-active crystals [1]. In this way, the CVL excitation threshold corresponds to the ionization energy of the outermost core state in the metal cation (E_{cc}, see figure 1). The range of the CVL emission spectrum reproduces the width of the valence band (ΔE_v), its low energy edge corresponds to the energy gap E_{g2} between

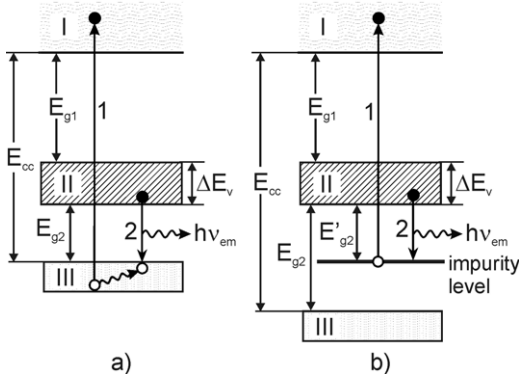

Figure 1. Scheme of the outermost energy bands for wide-band ionic crystals presenting absorption (1) and radiative (2) transitions corresponding to the intrinsic (a) and impure (b) core–valence luminescence (I—conduction band, II—valence band, III—outermost core band).

the bottom of the valence band and the outermost core state, and the high energy edge is the $E_{g2} + \Delta E_v$ value (see figure 1). Hence, the band gap E_{g1} may be expressed in terms of E_{cc}, ΔE_v and E_{g2} as

$$E_{g1} = E_{cc} - (E_{g2} + \Delta E_v). \tag{1}$$

Thus, the investigation of core–valence luminescence may be rather helpful when neither experimental nor theoretical data on the energy band structure are available.

The CVL is observed only if the energy of the core-to-valence transition is less than the band gap E_{g1} ($h\nu_{em} < E_{g1}$). One can meet this condition mostly in the case of halide crystals containing Cs^+, Rb^+, K^+ ions. The crystals of BaF_2, CsF, RbF, CsCl and CsBr are examples of CVL-active materials. The relaxation of outermost core holes occurs via Auger decay if the $h\nu_{em} < E_{g1}$ condition is not satisfied. In this case, the energy of core–valence recombination is absorbed by the valence electron and its further transition into the conductive band occurs.

Figure 1(b) presents the model of the outermost energy bands for the case when CVL is not observed because of the $h\nu_{em} > E_{g1}$ condition. The condition $h\nu_{em} < E_{g1}$ for the radiative core–valence recombination can be presented as $h\nu_{em} = E_{cc} - E_{g1} < E_{g1}$; hence $E_{cc} < 2E_{g1}$ is one of its commonly known forms. RbCl and KCl crystals are examples of halides that do not possess the intrinsic CVL. However, the CVL can be observed for RbCl and KCl crystals doped with Cs^+ ions [4, 5] introducing 5p Cs^+ core states with an ionization energy (E_{cc}) lower than that of the 4p Rb^+ and 3p K^+ host core. In this case, the radiative recombination involves the host valence electron and the core hole of the impurity cation. Such core–valence radiative recombination involving the impurity core states is known as impurity CVL and provides the possibility of extending the family of CVL-active materials [1]. The excitation threshold of impurity CVL corresponds to the ionization energy of the impurity cation core (figure 1(b), transition 1). Thus, the study of the impurity CVL can be considered as a method for the determination of the outermost energy band structure for crystals that do not reveal intrinsic CVL.

Among the $ACaCl_3$ (A = Cs, K, Rb) perovskite series, only $CsCaCl_3$ reveals intrinsic CVL [6, 7]. The impurity CVL is observed for the doped $RbCaCl_3$:Cs^+ and $KCaCl_3$:Cs^+ crystals [4]. Study of the intrinsic CVL in $CsCaCl_3$ and the impurity CVL in Cs^+ doped $RbCaCl_3$ and $KCaCl_3$ crystals facilitates the exploration of their energy band structures providing the initial and check parameters for the theoretical modelling.

To elucidate the energy band structure as well as the features of the intrinsic and impurity CVL of $A_{1-x}Cs_xCaCl_3$ (A = K, Rb) crystals, a luminescence spectroscopy study of $CsCaCl_3$, $Rb_{1-x}Cs_xCaCl_3$, $K_{1-x}Cs_xCaCl_3$ has been performed together with a theoretical calculation of the $CsCaCl_3$ energy band structure using the pseudopotential method taking into account the gradient corrections for the exchange–correlation energy [8].

2. Experiment details

Single crystals of $CsCaCl_3$, $Rb_{1-x}Cs_xCaCl_3$ and $K_{1-x}Cs_xCaCl_3$ ($x = 0.007$, 0.04, 0.1) were grown in quartz ampoules using the Stockbarger technique. The concentration of Cs^+ impurity (x values) has been controlled only in the respective raw melts.

Luminescence spectroscopy studies were performed at the Deutsches Elektronen Synchotron (DESY, Hamburg) using the facility of the SUPERLUMI station at HASYLAB [9]. A helium flow type cryostat has been used to carry out the measurements at $T = 8$ K. The time-resolved spectroscopy technique has been applied to extract the fast emission component corresponding to the core–valence luminescence. Emissions were analysed within the 200–600 nm range using the ARC 'Spectra Pro 308' 30 cm monochromator in a Czerny–Turner mounting equipped with a HAMAMATSU R6358P photomultiplier. Luminescence excitation spectra were scanned with the resolution of 3.2 Å within 10–30 eV using the primary 2 m monochromator in a 15° McPherson mounting.

3. The evaluation of the electronic energy bands and the density of states

The electron energy spectrum of a crystal $\varepsilon_{n\mathbf{k}} = \varepsilon_n(\mathbf{k})$ in band number n was found at the $\mathbf{k}$ point of the first Brillouin zone as a solution of the Kohn–Sham equation, given in the momentum representation:

$$\sum_{\mathbf{G}'}\left(\tfrac{1}{2}(\mathbf{k}+\mathbf{G})^2\delta_{\mathbf{G},\mathbf{G}'} + V_{\mathrm{H}}(\mathbf{G}-\mathbf{G}') + V_{\mathrm{xc}}(\mathbf{G}-\mathbf{G}') + V^{\mathrm{ps}}_{\mathrm{loc}}(\mathbf{G}-\mathbf{G}') + V^{\mathrm{ps}}_{\mathrm{nloc}}(\mathbf{k}+\mathbf{G},\mathbf{k}+\mathbf{G}')\right)c_{n\mathbf{k}}(\mathbf{G}') = \varepsilon_{n\mathbf{k}}c_{n\mathbf{k}}(\mathbf{G}), \tag{2}$$

where the first term is the kinetic energy, V_{H} is the Coulomb potential of electrons (Hartree potential), V_{xc} is the exchange–correlation potential depending on the electron density, $V^{\mathrm{ps}}_{\mathrm{loc}}$ is the local and $V^{\mathrm{ps}}_{\mathrm{nloc}}$ the non-local part of the pseudopotential. The unknown pseudowavefunction of an electron in a crystal is

$$\Psi_{n\mathbf{k}}(\mathbf{r}) = \frac{1}{\sqrt{\Omega}}\sum_{\mathbf{G}} c_{n\mathbf{k}}(\mathbf{G})\mathrm{e}^{\mathrm{i}(\mathbf{k}+\mathbf{G})\mathbf{r}}, \tag{3}$$

where Ω is a crystal volume and $\mathbf{G}$ denotes the reciprocal space vector.

The Hartree potential is given by

$$V_{\mathrm{H}}(\mathbf{G}) = \frac{4\pi\rho(\mathbf{G})}{\mathbf{G}^2}, \tag{4}$$

where the electronic density is calculated as

$$\rho(\mathbf{G}) = \frac{1}{\Omega}\sum_{n\mathbf{k}}\sum_{\mathbf{G}'} c_{n\mathbf{k}}(\mathbf{G}+\mathbf{G}')c^*_{n\mathbf{k}}(\mathbf{G}'). \tag{5}$$

The exchange–correlation potential V_{xc} is derived as the functional derivative of the generalized gradient approximation (GGA) for the exchange–correlation energy E_{xc} suggested by Perdew *et al* [8]:

$$V_{\mathrm{xc}}(\mathbf{r}) = \frac{\delta E_{\mathrm{xc}}}{\delta\rho(\mathbf{r})} - \nabla\frac{\delta E_{\mathrm{xc}}}{\delta\nabla\rho(\mathbf{r})}, \qquad E^{\mathrm{GGA}}_{\mathrm{xc}}(\rho) = \int \mathrm{d}\mathbf{r}\, f^{\mathrm{GGA}}_{\mathrm{xc}}(\rho(\mathbf{r}), \nabla\rho(\mathbf{r})). \tag{6}$$

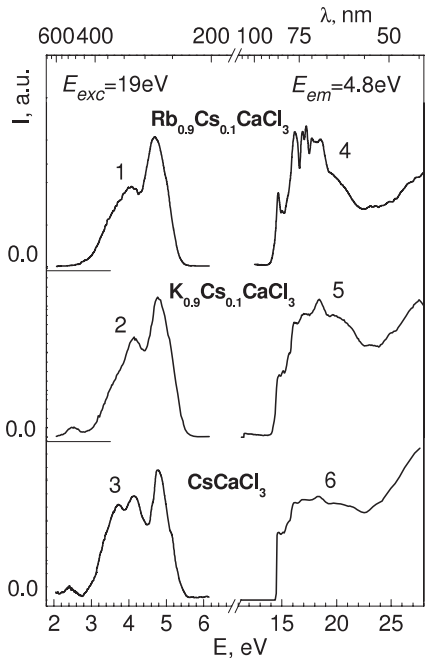

Figure 2. Emission (1, 2, 3) and excitation (4, 5, 6) spectra measured for the fast luminescence of $Rb_{0.9}Cs_{0.1}CaCl_3$, $K_{0.9}Cs_{0.1}CaCl_3$ and $CsCaCl_3$ crystals at $T = 8$ K.

The eigenvectors $c_{n\mathbf{k}}$ evaluated from the system of equation (2) are used for making the next steps of iterations. First the density of electrons is calculated on a grid in a direct space $\rho(\mathbf{r}_i)$ and then the potentials V_{H} and V_{xc} are evaluated. The matrix elements of V_{xc} in the momentum representation are calculated by means of the fast Fourier transformation (FFT) [10]. The pseudopotential parameters and the matrix elements of the local and non-local parts of the pseudopotential V^{ps} are given in direct and reciprocal space [11]. The iteration cycles were performed until the convergence in energy was achieved with tolerance 10^{-6} eV. The grid in direct and reciprocal space was $6 \times 6 \times 6$. The number of plane waves in (3) was defined by the cut-off energy $E_{\mathrm{cut}}^{\mathrm{PW}} = 850$ eV.

After reaching self-consistency the partial density of the electronic states in band number t was calculated by means of the formula

$$n_t(E) = \frac{\Omega_{\mathrm{c}}}{4\pi^3\sqrt{\pi}\sigma_t}\int \mathrm{d}\mathbf{k}\,\mathrm{e}^{-\left(\frac{E-E_t(\mathbf{k})}{\sigma_t}\right)^2}, \tag{7}$$

where σ_t is the factor of energy level smearing, Ω_{c} is the volume of the primitive cell.

4. Results and discussion

4.1. CVL spectra

Perovskite $CsCaCl_3$ crystal reveals the intrinsic CVL [6, 7]. This feature enables us to compare the simulated energy band structure of $CsCaCl_3$ with the experimental results on the energy band parameters obtained from the analysis of $CsCaCl_3$ CVL spectra. The measured CVL emission and excitation spectra (figure 2, curves 3, 6) reproduce the main features of their literature analogues [6, 7]. The excitation spectrum (curve 6) reveals the characteristic threshold

Table 1. The calculated and experimental data on the structure of the outermost energy bands for $CsCaCl_3$ and $A_{1-x}Cs_xCaCl_3$ (A = K, Rb) crystals.

	$CsCaCl_3$		$Rb_{0.9}Cs_{0.1}CaCl_3$	$K_{0.9}Cs_{0.1}CaCl_3$
	Theory (eV)	Experiment (eV)	Experiment (eV)	Experiment (eV)
E_{cc}	10.1	14.3	14.0	14.0
E_{g1}	5.0	8.6	8.4	8.3
E_{g2}	2.7	2.9		
ΔE_v	2.4	2.8	2.7	2.8
$\Delta E_v + E_{g2}$	5.1	5.7		

at 14.3 eV corresponding to the ionization of the outermost 5p Cs^+ core states. Table 1 presents the parameters of the energy band structure estimated for $CsCaCl_3$ and $A_{1-x}Cs_xCaCl_3$ (A = K, Rb, $x = 1, 0.1$) crystals from their CVL spectra.

The emission bands are peaked at 4.6, 4.0 eV for $Rb_{0.9}Cs_{0.1}CaCl_3$ (figure 2, curve 1) and at 4.7, 4.1 eV for $K_{0.9}Cs_{0.1}CaCl_3$ (curve 2), in some agreement with the emission bands of the $CsCaCl_3$ CVL (curve 3). However, there is no evidence for $CsCaCl_3$ phase formation in Cs^+ doped $RbCaCl_3$ and $KCaCl_3$ crystals because the excitation and CVL spectra are similar for all concentrations of the Cs impurity ($x = 0.007, 0.04, 0.1$) in $A_{1-x}Cs_xCaCl_3$ (A = K, Rb) crystals. Moreover, the formation of a continuous solid solution series is known for ABX_3 perovskite crystals upon the substitution of either B or A cations. The series of $Rb_{1-x}K_xCaF_3$ crystals can be considered as a characteristic example of such solid solution series. The existence of a continuous $Rb_{1-x}K_xCaF_3$ solid solution series has been proved by neutron scattering experiments [12] and electron paramagnetic resonance study [13]. Thus, we can conclude the existence of continuous solid solution series for $A_{1-x}Cs_xCaCl_3$ (A = K, Rb) crystals. In this case, the CVL of Cs^+ doped $RbCaCl_3$ and $KCaCl_3$ is due to the radiative recombination of valence electrons with the impurity 5p Cs^+ core holes, but does not originate from the core–valence transitions within the $CsCaCl_3$ cluster embedded in $RbCaCl_3$ and $KCaCl_3$ hosts. Thus, the luminescence of $Rb_{1-x}Cs_xCaCl_3$ and $K_{1-x}Cs_xCaCl_3$ (figure 2, curves 1, 2) observed upon 5p Cs^+ core ionization may be attributed to the impurity CVL.

The excitation spectra of $Rb_{0.9}Cs_{0.1}CaCl_3$ and $K_{0.9}Cs_{0.1}CaCl_3$ CVL reveal rather pronounced thresholds at $E_{cc} = 14.0$ eV followed by well resolved peaks within the 14.5–19.0 eV range and rising efficiency after $E > 22$ eV. The excitation 14.3 eV threshold of $CsCaCl_3$ fast emission is related to 5p Cs^+ core hole creation and coincides with the respective excitation thresholds for $Rb_{1-x}Cs_xCaCl_3$ and $K_{1-x}Cs_xCaCl_3$ crystals (figure 2). Therefore, the fast emission registered for $Rb_{1-x}Cs_xCaCl_3$ and $K_{1-x}Cs_xCaCl_3$ within the 3–6 eV range is the impurity CVL originating from the radiative recombination of 5p Cs^+ core holes with valence electrons.

4.2. Energy structure

Features of the intrinsic CVL spectra of $CsCaCl_3$ are well reproduced in the case of impurity CVL of $Rb_{1-x}Cs_xCaCl_3$ and $K_{1-x}Cs_xCaCl_3$ (figure 2) which implies similarity in structure of the outermost energy bands for these crystals. $RbCaCl_3$ and $KCaCl_3$ crystals have the D_{2h}^{16} symmetry space group, whereas O_h^1 is known for $CsCaCl_3$ with lattice parameter $a = 5396$ Å and it is therefore easier to simulate the energy band structure for $CsCaCl_3$ than for $RbCaCl_3$ and $KCaCl_3$. Here, the CVL spectra crystals were compared with the results from energy band simulation restricted to $CsCaCl_3$.

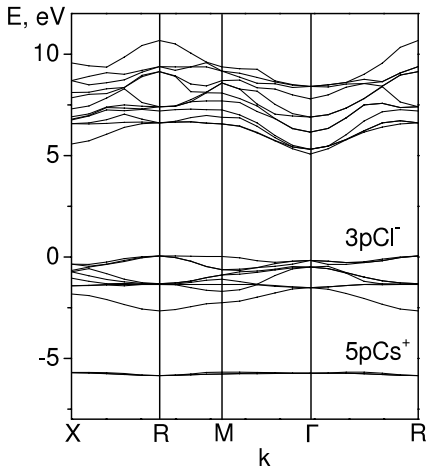

Figure 3. The energy band scheme for the $CsCaCl_3$ crystal.

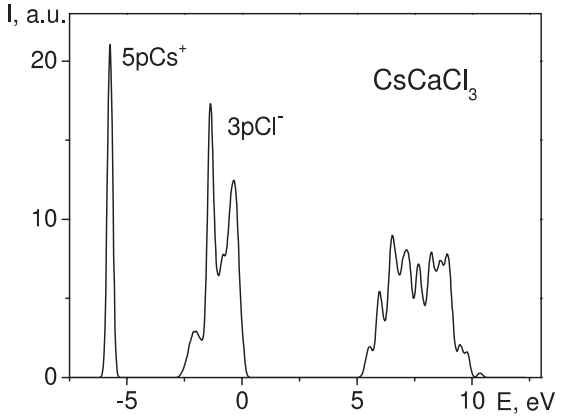

Figure 4. Distribution of the general density of electron states for $CsCaCl_3$ crystals.

The calculated $CsCaCl_3$ energy band structure (figure 3) shows the major contribution of 3p Cl^- states to the valence band and the location of 5p Cs^+ states in the outermost core band within $-(6.0–5.3)$ eV. According to the calculation, the energy gap E_{g2} between the valence 3p Cl^- and core 5p Cs^+ states is 2.7 eV and the width of the valence band ΔE_v is 2.4 eV (table 1).

For the elucidation of the energy band structure, the partial density of electron states has been calculated according to the formula (7). The main contribution to the density of valence electron states is provided by the p states of Cl^-, whereas the partial density of s and d states is an order of magnitude smaller. The structure of the valence band is therefore defined by the density of 3p Cl^- states. The general density distribution for the electron states of $CsCaCl_3$ is presented in figure 4 as the sum of partial densities for all electron states. The general density of valence electron states reveals main maxima at -2.1, -1.3 and -0.4 eV.

The valence and core electron states are mostly of p type. Since the p–p transitions are forbidden the radiative decay of 5p Cs^{2+} holes should occur due to s–p and d–p valence-to-core electron transitions. In this case the structure of the CVL emission spectrum should reproduce the cumulative density of s and d electron states in the valence band [14]. Figure 5 presents

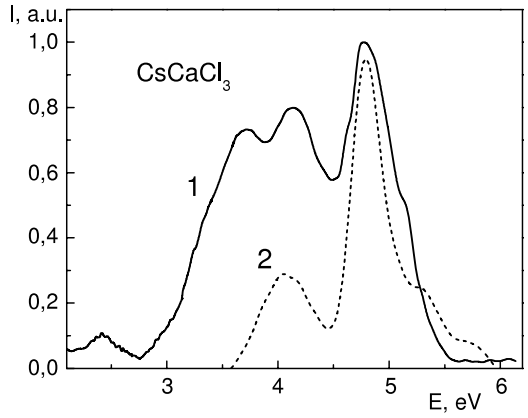

Figure 5. CVL emission spectrum (curve 1) and the cumulative density of valence s and d electron states (curve 2) of the $CsCaCl_3$ crystal.

the comparison of the $CsCaCl_3$ CVL emission spectrum (curve 1) with the cumulative density of valence s and d electron states calculated with the smearing factor $\sigma_t = 0.1$ eV (curve 2). Some similarity between the simulated density of valence s, d states and the experimental emission spectrum of $CsCaCl_3$ (figure 5) may partly confirm our assumption as regards the type of electron valence-to-core radiative transitions giving rise to the CVL phenomenon.

The understated value (5.0 eV) of the E_{g1} gap (table 1) is caused by the neglect of energy changing of the core level position under the transition from free ion to crystal, i.e. the pseudopotential for the crystal has been formed considering the core level position for free ions (2).

The similarity of the intrinsic CVL spectra of $CsCaCl_3$ and the impurity CVL of $Rb_{1-x}Cs_xCaCl_3$ and $K_{1-x}Cs_xCaCl_3$ implies similar structures of their outermost energy bands and validates the structure of $CsCaCl_3$ energy bands (figure 3) as being suitable for the interpretation of optical band-to-band transitions in $RbCaCl_3$ and $KCaCl_3$ as well.

5. Conclusions

The CVL spectra of $CsCaCl_3$, $Rb_{1-x}Cs_xCaCl_3$ and $K_{1-x}Cs_xCaCl_3$ crystals reveal rather similar features, validating the assumption of similar structures of their outermost energy bands. The structure of the outermost energy bands has been calculated for $CsCaCl_3$ crystals using the pseudopotential method with gradient corrections of the exchange–correlation energy. Similarity in structure of the CVL emission spectrum and the calculated density of valence s and d states assumes a major contribution of s–p and d–p electron valence-to-core radiative transitions to the radiative decay of 5p Cs^{2+} holes. Differences between some of the calculated and experimental parameters appear due to the peculiar formation of the pseudopotential in the crystal.

Acknowledgments

The authors are grateful to Professor G Zimmerer from Hamburg University for allowing use of the SUPERLUMI station for synchrotron radiation measurements. The work was partially supported by Ukraine Ministry of Science and Education (grant no. 0106U001287).

References

[1] Rodnyi P A 1997 *Physical Processes in Inorganic Scintillators* (New York: CRC Press) p 219
[2] Makhov V N, Kuusmann I, Becker J, Runne M and Zimmerer G 1999 Crossluminescence at high temperatures *J. Electron. Spectrosc. Relat. Phenom.* **101–103** 817–20
[3] Mikhailik V B, Itoh M, Asaka S, Bokumoto Y, Murakami J and Kamada M 1999 Amplification of impurity-associated Auger-free luminescence in mixed rubidium–caesium chloride crystals under core-level excitation with undulator radiation *Opt. Commun.* **171** 71–6
[4] Voloshinovskii A 2001 Decay of 5p Cs-core excitations in halide crystals with core valence luminescence *Radiat. Meas.* **33** 565–9
[5] Mikhailik V B, Voloshinovskii A S and Zimmerer G 1999 Core–valence luminescence as a method of studying the relaxation processes in the outermost core of the crystal *J. Alloys Compounds* **286** 128–36
[6] Melchakov E N, Rodnyi P A, Rybakov B N, Smakov A N and Terekhin M A 1989 *Fiz. Tverd. Tela* **31** 276–8
[7] Kamenskikh I A, MacDonald M A, Mikhailin V V, Munro I H and Terekhin M A 1992 Cross luminescence of several perovskite-type crystals *Rev. Sci. Instrum.* **63** 1447–9
[8] Perdew J P, Burke K and Ernzerhof M 1996 *Phys. Rev. Lett.* **77** 3865–8
[9] Zimmerer G 1991 Status report on luminescence investigations with synchrotron radiation at HASYLAB *Nucl. Instrum. Methods* **308** 178–86
[10] Press W H, Flannery B P, Teukolsky S A and Vetterling W J 1989 *Numerical Recipes* (Cambridge: Cambridge University Press)
[11] Hartwigsen C, Goedecker S and Hutter J 1998 *Phys. Rev.* B **58** 3641–62
[12] Rousseau M, Daniel Ph, Toulouse J and Hennion B 1997 *Physica* B **234–236** 139–41
[13] Buzare J Y and Foucher P 1991 *J. Phys.: Condens. Matter* **3** 2535–44
[14] Voloshinovskii A S, Mikhailik V B, Rodnyi P A, Syrotyuk S V, Shpak A P and Yaresko A N 1994 *Phys. Solid States* **36** 911–3